Event-based 3d-Lagrangian Particle Tracking using Different Processing Strategies

Christian Willert[1,*], Sebastian Sachs[2,4], Daniel Schanz[3], Christian Cierpka[2], Massimiliano Rossi[4], Gabriele Bellani[4]

1: Institute of Propulsion Technology, German Aerospace Center (DLR), Köln, Germany
2: Institute of Thermodynamics and Fluid Mechanics and Institute of Micro- and Nanotechnologies, Technische Universität Ilmenau, Ilmenau, Germany
3: Institute of Aerodynamics and Flow Technology, German Aerospace Center (DLR), Göttingen, Germany
4: Department of Industrial Engineering / CIRI Aerospace, University of Bologna, Forlì, Italy

*Corresponding author: chris.willert@dlr.de

Keywords: fluid flow measurement, particle imaging, event-based imaging, dynamic vision sensor, particle tracking, PTV, “Shake-the-Box” algorithm, STB

ABSTRACT

Image-based measurements in turbulent flows, where high magnification is often required to preserve spatial resolution, leads to particle displacements of several 100,000 pixels per second and requiring fast cameras for time-resolved observation. Since turbulence is three-dimensional, multiple synchronized cameras are needed to resolve volumetric particle motion. For statistically converged measurements over several minutes, conventional frame-based high-speed systems can generate data volumes of $O(10\,\mathrm{Terabyte})$ and require costly cameras and high-power laser light sources. Event-based cameras, combined with continuous-wave laser illumination, offer a potential alternative with substantially reduced cost and data volume, but introduce specific processing challenges to be addressed. In the present work, we describe different strategies to retrieve time-resolved particle tracking data from event-based particle imagery acquired with multiple synchronized event cameras in a multi-view arrangement. Continuous and pulsed illumination are compared, as they offer complementary advantages for particle tracking. Measurements are performed in the viscous sublayer of a flat-plate boundary layer and of turbulent pipe flow in the high-Reynolds-number CICLoPE Long Pipe facility. The different processing pipelines enable the reconstruction of time-resolved 3D trajectories, namely the open-source STELLA framework and the Shake-The-Box. Their respective benefits and limitations are discussed. In particular, the application of Shake-The-Box particle tracking to single-timestep pseudo-images from pulsed illumination is shown to be feasible after suitable preprocessing. Gaussian smoothing transforms the binary pseudo-images into a format compatible with standard peak-detection and position-optimization schemes used within STB. In contrast, STELLA works directly at the sparse event stream from the cameras. The results demonstrate the potential of event-based volumetric tracking for near-wall turbulence measurements, while further datasets and improved experimental conditions are required to assess tracking stability and accuracy under varying flow and illumination conditions.

1. Introduction

Event-based vision (EBV), also termed *dynamic vision sensing* (DVS), is a new imaging approach that recently has garnered increased attention within the field of computer vision as it offers a combination of low data rate (compressed sensing) and high temporal resolution. Underlying concepts of EBV and its current state of technology are reviewed by Gallego et al. [4]. Contrary to conventional frame-based imaging, EBV only records changes of image intensity (i.e. contrast changes) on the pixel level, triggering a positive event for increasing intensity and a negative event for a decreasing intensity change. The typical threshold of the intensity-change trigger is on the order of 10–20%, but can be fine tuned. As the pixels on the detector respond individually, the events appear asynchronously throughout the detector area resulting in a continuous stream of data, with each event datum consisting of pixel coordinates, a time stamp and a polarity indicating the direction of the intensity change.

The present work describes the extension of event-based imaging velocimetry to 3d Lagrangian Particle Tracking [13]. Previous work was performed by Drazen et al. [3] on particle tracking velocimetry (PTV) of dense particle distributions in a solid–liquid two-phase pipe flow using an EBV sensor of 256×256 pixels and cw-laser (5W) illumination. A stereoscopic EBV system was used by Wang et al. [15] to reconstruct three-dimensional tracks from 2d tracking results from each camera. First PTV measurements in an air flow were performed by Borer et al. [2] using three synchronized EBV cameras (128×128 pixels) to track helium filled soap bubbles (HFSB) in volumes up to about 1 m side length using white light LED arrays for illumination. The flow was only sparsely seeded allowing individual particles to be tracked with final data sets containing up to $O(1\,000$ - $10\,000)$ tracks. Rusch & Rösgen [9] re-implemented this concept as a real-time 3d PTV system enabling live flow field reconstruction.

More recently, Willert & Klinner [19] implemented a triple-event-camera setup to perform near-wall PTV within the viscous sublayer of a turbulent boundary layer using a thin laser light sheet. By recording long records of up to one minute duration, converged velocity and wall-shear stress statistics could be obtained. Track reconstruction was based on photogrammetric matching of the individual tracks from different views, an approach that typically is limited to sparsely seeded flows. Considerably improved tracking performance at higher seeding densities can be achieved with the recently introduced and now well established Shake-the-Box (STB) Lagrangian tracking method [11]. The present work describes both the extension of STB to event-based imagery as well as the extension of the 2d tracking approaches laid out by Sachs et al. [10] to 3d*.

To date, the literature has not reported on the synchronized operation of four or more event cameras which is recommended for reliable performance of the STB algorithm. Along with this the authors have already demonstrated that high particle image densities are feasible with EBV [18, 8]. The purpose of the present work is to assess the performance and limitations of event-based STB and related particle tracking techniques on canonical flows such as the turbulent boundary layer

*The STELLA software is openly available at `https://github.com/sesa1504/STELLA`

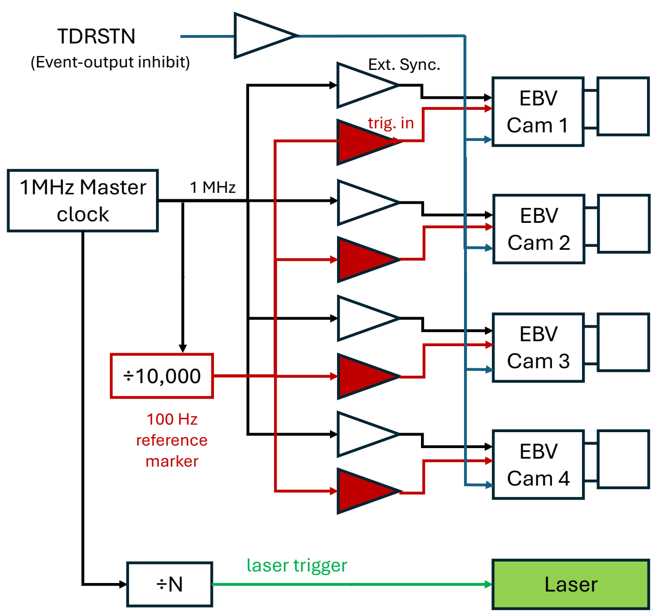

Figure 1. Synchronization scheme for multiple event cameras using a microcontroller (PRJC Teensy 4.1) to provide a 1 MHz common clock to all event-cameras. Laser pulsing is synchronized to the same clock. Simultaneous camera streaming is initiated by a an externally provided, common pixel-reset signal (TDRSTN).

along a flat plate or within a turbulent pipe flow.

2. Implementation

2.1. 3d-3c Tracking System

The herein used 3d-3c particle tracking system consists of four event-based cameras (IDS uEye XCP-E/UE-39B0XCP-E) in a photogrammetric configuration, that is, arranged in a manner to capture a common volume of interest. The cameras are externally synchronized with a common 1 MHz signal from a microcontroller (see Fig. 1). The same device also provides a reference pulses at defined, low frequency intervals to allow a 1 µs precise alignment of the acquired event records with respect to each other. A common event-output inhibit signal (TDRSTN) ensures that all cameras start streaming at the same time. All event cameras are connected via USB3.1 (5 Gbps) interface cables to a single host computer that is able to handle a sustained data stream of 4×100 MB/s which corresponds to about 50×10^6 events/s per camera. Experiment specific aspects of the measurement setup are given in the following sections.

2.2. Camera calibration

Essential for reliable 3d particle image reconstruction is a camera calibration that provides accurate mappings between image and object space. While a single view of a planar calibration target may be sufficient to obtain camera pose [17], the herein used camera calibration relies on multiple images of a z-translated calibration target. In practice, chemically etched chrome-on-glass lithographic targets are mounted on a microtraverse. The calibration pattern consists of either a checker-board pattern or a regular grid of small dots (apertures). With the event cameras only responding to intensity changes, the stationary target is back-illuminated by a pulsed light source to generate a suited event stream. Summing the events over several seconds results in pseudo-images of the target that can be processed with conventional (PIV) camera calibration software. Reference markers retrieved from the calibration target images provide the object–image point correspondences that form the basis for camera calibration.

The chosen camera model is based on a direct linear transform (DLT) which is linear mapping involving a 3×4 projection matrix between 2d image coordinates and 3d object space. The model does not account for any distortions introduced by the imaging lens or windows. If necessary, residual camera view misalignment is accounted by disparity correction using the particle images themselves, as is common practice in STB processing [12].

The combined views of all four cameras using DLT mappings obtained by point correspondence from 5 z-translated target images are shown in Fig. 2a and b for the measurement setups described in Sec. 3.1 and 3.2, respectively.

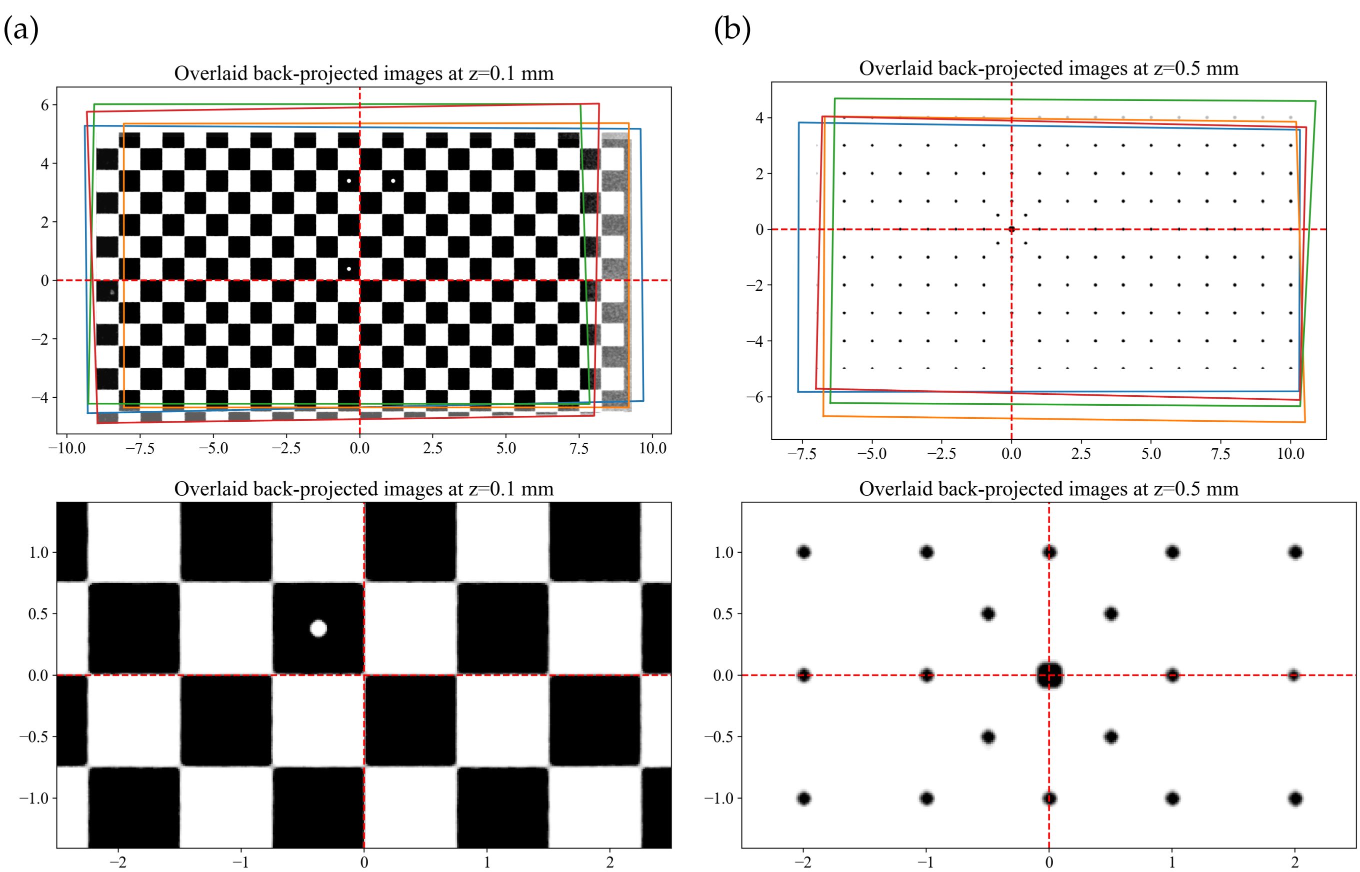

Figure 2. Back-projected images of calibration targets obtained in the measurement setups described in Sec 3.1 (a) and 3.2 (b) based on camera calibration employing the DLT camera model. Magnified details are shown below. Colored lines outline the actual field of view of the respective cameras.

2.3. Tracking methodology

Two different tracking approaches will be pursued: a 3d matching of continuous 2d tracks extracted by the STELLA algorithm [10] and Shake-The-Box [11], relying on evaluating time-series of pseudo-images obtained by illuminating the volume with a pulsed light source.

3d PTV based on continuous 2d particle tracking

Continuously illuminated particles leave a characteristic footprint in the obtained event stream, akin to particle tracing images, which can be processed directly to extract 2d-2c particle tracks in each camera view [10]. This omits the accumulation of events into pseudo-images for particle identification. Based on the camera calibration using DLT, detected 2d tracks from different camera views are paired to allow for a reconstruction of the track in space. Due to the individual latency of each camera depending on light conditions, event rate, and camera settings, an adjustable time window is defined to achieve reliable track pairings. Following an outlier detection to reject tracks containing nonphysical spatial discontinuities, 3d-3c tracks are refined by applying a hybrid approach of Kalman filtering and spline fitting [10].

The 3d track reconstruction strategy from multi-view 2d-2c tracking results can be outlined as follows:

1. For each view, sample 2d tracks with short time-windows (typically $250\,\mu s$ to $1000\,\mu s$); this will provide sub-sets of short tracklets.
2. Compute the mean positions of the tracklets in each view.
3. Use a search domain on epipolars to match the mean locations of tracklets in the other views.
4. Matched tracklets form a new 3d track consisting of the original track data $(x, y, t)_i$ from each available view.
5. Using unique IDs for each 2d track, the 3d track reconstruction can be extended beyond the current time window.
6. For the following time-intervals, the time-sampling and position averaging procedure in step 1 is repeated for 2d tracks not yet assigned to 3d tracks. Broken tracks are efficiently handled through this approach.

Shake-The-Box

STB applies iterative particle reconstruction (IPR) [16, 6] to reconstruct 3d particle clouds from image time-series of several cameras using triangulation approaches. Once a preliminary tracking system is established, STB relies on an extension of the known tracks to the next time-step. For this, a predictor/corrector scheme is applied, where the known tracks at time-step t_i are extrapolated to t_{i+1}. The prediction is followed by a position optimization step, which iteratively shifts each predicted particle to the position best matching the local particle images on all cameras at t_{i+1}. This optimization step, often referred to as “shaking” the particles, operates on the gradient of a cost function that is determined via the sum of the local residual intensities on all cameras. For the standard STB implementation, working on normal camera images, the gradient can be accurately determined due to the Gaussian shape of the particle images. Single-time-step Pseudo-images gained from EBV pose several challenges to this scheme. A Gaussian shape is not present in the aggregated images with pulsed illumination, where particle images are flat-top circles, ellipses or even crescent-shaped, depending on the imaging conditions. This effectively inhibits the successful identification of the particle image peaks required for the triangulation process. A reliable determination of the cost function used for position optimization is also inhibited. As will be shown in the results section, applying simple Gaussian smoothing to such binary images is a viable way of alleviating the mentioned problems with Event-based pseudo-images. However, more advanced alternatives – adapted to the nature of the EBV data – should be explored in the future.

3. Measurement configurations

Event-based image data is acquired from two different flow facilities with similar imaging configurations involving four event-cameras. In both cases – a flat plate and a circular pipe – the near-wall turbulent flow is imaged with high magnification to capture the dynamics within the viscous sublayer and slightly above.

3.1. Flat plate turbulent boundary layer

Flat plate turbulent boundary layer (TBL) measurements are performed in the 1 meter wind tunnel (1mWK) of the DLR Institute of Aerodynamics and Flow Technology in Göttingen.

A schematic of the camera and laser arrangement is outlined in Fig. 3. The near-Gaussian shaped beam of a pulsed laser (Innolas Photonics/Iradion, Nanio-Air-532-SP) is formed into a thin light sheet and introduced from the side of the windtunnel test section at an angle of 0.5° to the test section wall. The illuminated volume of roughly $16 \times 7.5 \times 0.5\,\mathrm{mm}^3$ is imaged through a $0.8\,\mathrm{mm}$ thin window from below by 4 event-cameras with 1280×720 pixel sensors (IDS Imaging, uEye UE-39B0XCP-E with Sony IMX636 sensor). The cameras are photogrammetrically arranged with about 30° between the viewing axes. Tilt-mounts ensure a nearly homogeneous focal plane across the oblique views. Three of the four cameras receive the light scattered by the particles at a nearly orthogonal light scattering direction, whereas the fourth camera (Cam.4) collects forward scattered light of higher intensity such that its lens aperture is reduced from $f/4$ to $f/5.6$.

The flow is seeded with glycerol-water droplets created by a stage fogger (HazeBase Classic, base*L fluid). The flow tracers, with an estimated size of $1\,\mu\mathrm{m}$ to $2\,\mu\mathrm{m}$, are introduced downstream of the measurement location and are allowed to circulate within the tunnel circuit several times to

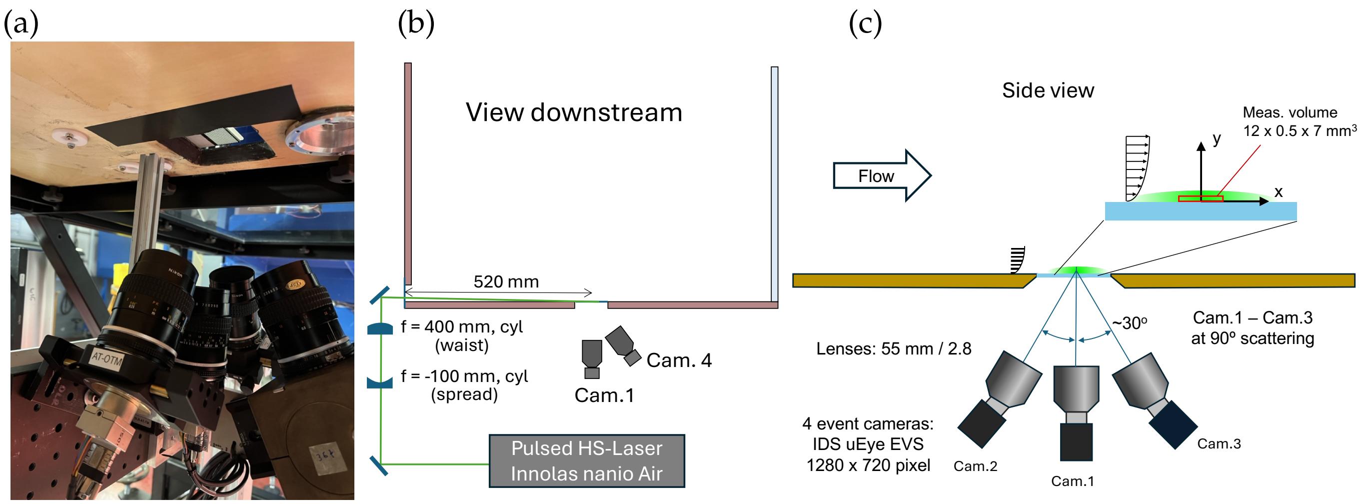

Figure 3. Photograph (a) and schematic (b,c) of four EBV camera configuration for near-wall EB-PTV in a turbulent boundary layer (TBL).

achieve a homogeneous distribution. The seeding concentration is varied through the duration of tracer supply. A slow evaporation rate ensures nearly stable seeding concentrations over several minutes.

Event-imaging records are acquired at three fixed wind tunnel flow velocities: $U_\infty = 3.4\,\mathrm{m/s}$ with a laminar boundary layer, $U_\infty = 4.0\,\mathrm{m/s}$ showing transitional flow, and $U_\infty = 5.2\,\mathrm{m/s}$ with a fully developed TBL ($\mathrm{Re}_\tau = 585$). Laser pulsing is increased from $2.5\,\mathrm{kHz}$ at the lower flow speed to $4.0\,\mathrm{kHz}$ to $5.0\,\mathrm{kHz}$ at the higher U_{cl}. For different seeding concentrations the event record length is varied between $5\,\mathrm{s}$ up to $30\,\mathrm{s}$.

3.2. Turbulent pipe flow

A second set of measurements was acquired in the Long Pipe faciility in CICLoPE (Center for International Cooperation in Long Pipe Experiments) of the University of Bologna in Forlì, Italy. The facility features a $111.15\,\mathrm{m}$ long pipe of $901\,\mathrm{mm}$ diameter in which dynamically and thermally stable flow conditions can be provided [1, 14]. The facility is designed to produce high Reynolds number flows ($5.000 < Re_\tau < 45.000$) while maintaining the viscous length scales l^* at a measurable level (>$10\ \mu$m).

The employed EB-PTV imaging setup, shown in Fig 4, is very similar to the previously described EB-PTV setup on the 1mWK and makes use of the same event-camera models (IDS Imaging, uEye UE-39B0XCP-E).

Macro lenses with a focal length of $105\,\mathrm{mm}$ (Nikon Mikro-Nikkor 105/2.8) allow a larger working distance at a similar optical magnification. The lens aperture is set to $f/5.6$. The near wall region is observed through a rectangular ($30\,\mathrm{mm} \times 32\,\mathrm{mm}$) window whose convex surface nearly matches the inner contour of the pipe (cylindrical lens of $f = -1000\,\mathrm{mm}$). To achieve a light sheet that

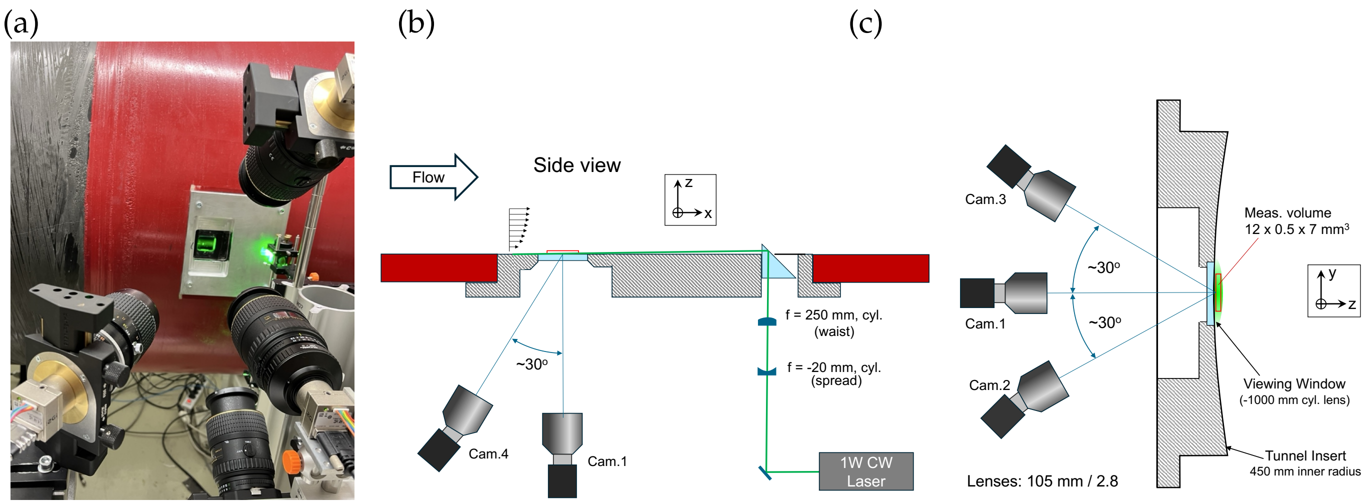

Figure 4. Photograph (a) and schematic (b,c) of four EBV camera configuration for near-wall EB-PTV of the TBL of the CICLoPE pipe facility.

is nearly parallel to the wall of the round pipe's geometry, the light sheet is introduced using a recessed right-angle prism located about 100 mm downstream of the measurement location and protruding about 5 mm into the flow. Careful alignment achieved a light sheet that leaves the prism less than 1 mm above the tunnel's inner contour with an incidence angle at the viewing window of less than 0.5°. With Cam.4 receiving stronger forward scattered light from the illuminated particles, its aperture is stepped down to match the intensity received by Cam.1 – Cam.3.

The same seeding methodology as in the previously described 1mWK setup is used. At varying seeding densities, records of up to 60 s are acquired, for both continuous as well as pulsed illumination, the latter achieved by modulation of the cw-laser at a frequency of 4 kHz. Due to the limited laser power (1.0 W) a rather long duty cycle of 25 % is required to achieve sufficient scattering intensity which results in minor streaking of faster moving particles.

4. Results

Fig. 5a and b respectively show events produced by continuous and pulsed illumination that are accumulated into pseudo-images and color-coded by the event recorded in the Long Pipe facility. Using either illumination strategy, coherent streamwise-oriented particle motion with elongated regions of different streamwise velocity are revealed, consistent with high- and low-speed streaks in the wall-parallel plane. Local variations in the spanwise particle motion reflect intermittent regions of pronounced in-plane shear associated with streak meandering.

In the magnified view of recordings with pulsed illumination at 4 kHz in Fig. 5d, the increasing particle image displacement between subsequent pulses indicates changes in the projected in-plane velocity observed in the single camera view. Considering that the thin light-sheet in the present configuration is entirely placed in the viscous sublayer, this behavior is consistent with particles sampling the strong streamwise wall-normal gradient while traversing in out-of-plane direction (*i.e.* with a Reynolds-stress producing event). The resulting lagrangian track can be resolved by combining the multi-camera views.

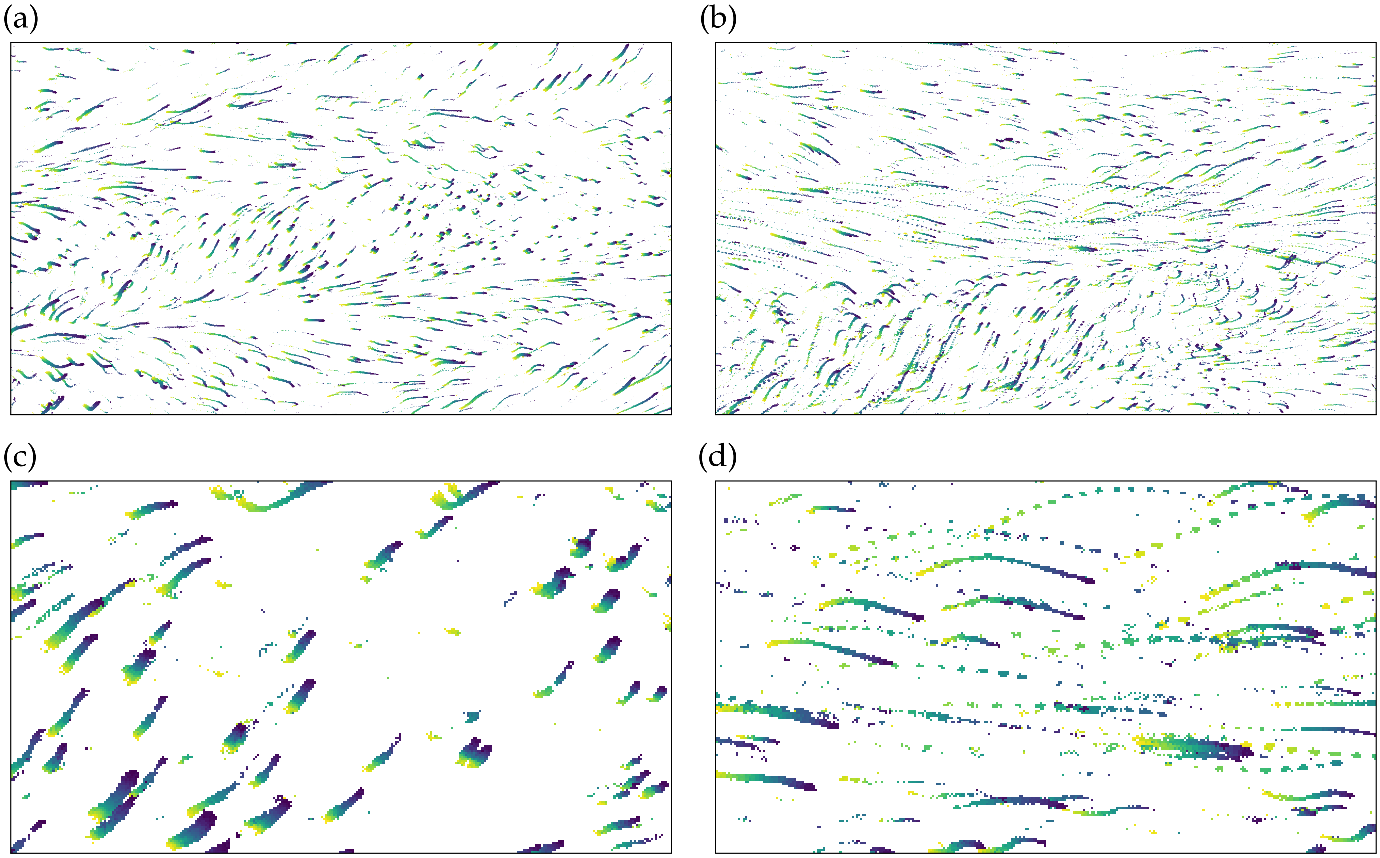

Figure 5. Pseudo-images of events from one camera color-coded by the event time for continuous illumination (a) and pulsed $4\,\mathrm{kHz}$ illumination (b) with magnified portion below (c,d). Flow is from left to right, recorded in the CICLoPE Long Pipe facility at a centerline velocity of $U_{cl} = 5\,\mathrm{m/s}$ ($\mathrm{Re}_\tau = 5000$); sample duration is $5\,\mathrm{ms}$. Event rate is $37 \times 10^6\,\mathrm{Ev/s}$ for both.

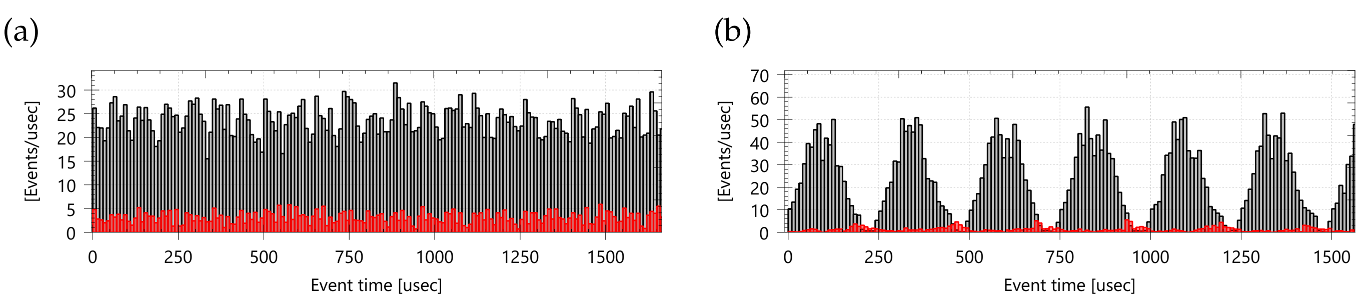

Figure 6. Event rate vs. time for continuous (a) and pulsed illumination (b) corresponding to data shown in Fig. 5. Bin-width is $10\,\mu\mathrm{s}$. Red markers (not-used in the processing) indicate negative events.

Differences in the event rate obtained by continuous and pulsed illumination are illustrated in Fig. 6a and b, respectively. While the average event rate remained similar in both measurements, a significantly higher peak in the event rate is evident using pulsed illumination. Furthermore, the temporal jitter in the recorded event timestamps becomes visible and was corrected by the known timing of the laser pulses. In both cases, negative events as highlighted in red are greatly suppressed by adjusting the camera settings and only positive events are utilized for particle tracking.

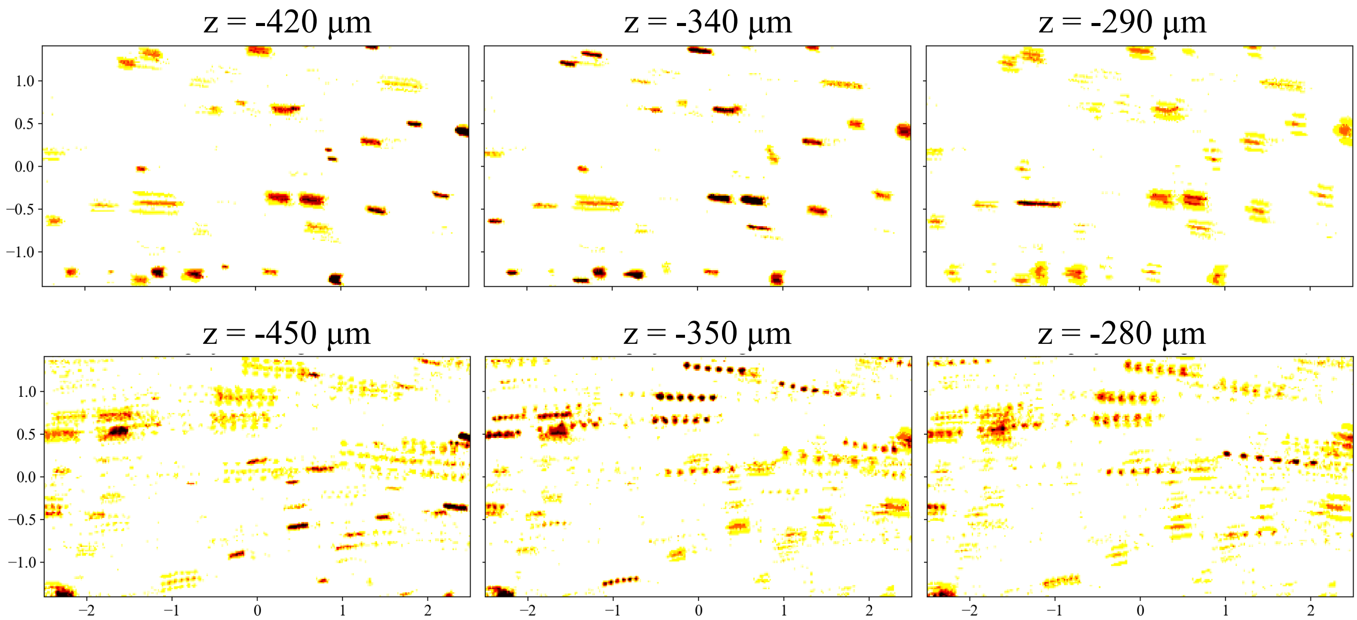

Figure 7. Sample of back-projected events from all four event cameras into object space at 3 different z-planes for $1\,\mathrm{ms}$ for continuous illumination (top row) and 6 light pulses ($1.5\,\mathrm{ms}$ duration, bottom row). Black intensity indicates overlap of events from all four cameras, red and orange indicate partial overlap. Axis scaling in mm. z-position is relative to calibration target.

Fig. 7 shows the back-projection of a short sample of events into object space at three different planes parallel to the calibration target. The back-projected events are yellow-colored. Twice overlapping events are orange, triple overlapped are red, switching to black if the events from all four cameras overlap in both space and time. Particles near the glass surface come into focus at $z \approx -450\,\mu\mathrm{m}$ while the faster particles can be tracked out to $z \approx -280\,\mu\mathrm{m}$ indicating a light sheet thickness of about $200\,\mu\mathrm{m}$, corresponding to approximately 2 wall-units at the present Reynolds number.

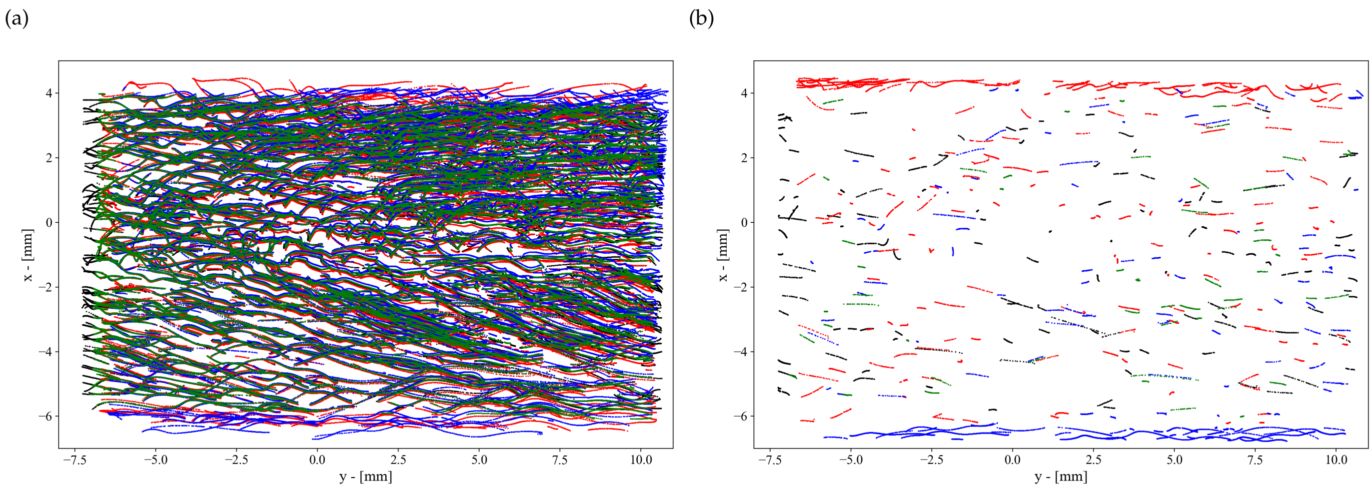

Figure 8. Matched tracks (a) and remaining tracks (b) for a $50\,\mathrm{ms}$ sample of 2d tracking results obtained with the STELLA algorithm.

The sample data in Fig. 7 confirm that accurate reconstruction at the $\mu\mathrm{m}$-scale is feasible even with 1-bit intensity streamed by event-cameras. In addition, most particles are simultaneously captured by a minimum of three cameras which enables a robust 3d reconstruction.

4.1. Reconstruction from 2d Tracking Data

Event-recordings obtained with continuous illumination at a pipe centerline velocity of $U_{cl} = 5\,\mathrm{m/s}$ is processed with the previously described reconstruction scheme. For each camera view the STELLA algorithm provides 2d-2c tracking results that are reconstructed using epipolar matching. 3d reconstruction of the $1\,\mathrm{s}$ long records is performed in overlapping chunks of $25\,\mathrm{ms}$ duration. To obtain velocity and acceleration data, the 3d points of the reconstructed tracks are spatially smoothed with a Gaussian filter of $\sigma = 10\,\mu\mathrm{s}$, although spline fitting and/or Kalman filtering may provide more robust estimates. The data points are weighted with the inverse of the reconstruction residual (mean $\approx 8\,\mu\mathrm{m}$). The 3d points are then (manually) aligned with the windtunnel surface and "flattened" in the spanwise direction to account for the curved inner surface. The projected ensemble of all reconstructed data points ($N \approx 5 \times 10^6$) onto the xz and yz-plane is shown in Fig. 9. The data points are clustered within a thin volume of about $100\,\mu\mathrm{m}$ thickness with a slight spanwise asymmetry induced by the non-uniform light distribution along the light sheet. Also the thickness, introduced from the left, of the sheet varies in streamwise direction x.

The aligned and rectified data is then bin-averaged using bins of $\Delta z = 2\,\mu\mathrm{m}$ thickness, rejecting data points with excessive acceleration $|a|_{\max} = 100\,\mathrm{m\,s^{-2}}$ and velocity $|u|_{\max} = 2\,\mathrm{m/s}$. Profiles of the mean velocity components and variances in the immediate proximity of the smooth wall are plotted in Fig. 10. The data is normalized by the mean friction velocity u_τ obtained through a linear least-square fit within a limited range of $0.5 < z^+ < 1.5$ where the profile exhibits a nearly linear trend. The fitting domain coincides with the sample count that reaches a maximum at $z^+ \approx 1.0$.

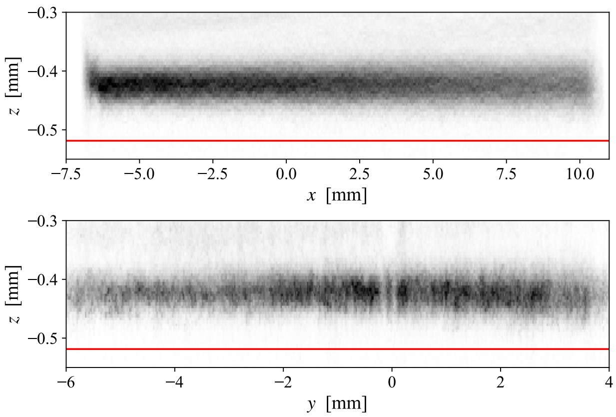

Figure 9. Projection of all data points reconstructed from $1\,\mathrm{s}$ of event data ($N \approx 5 \times 10^6$ at a pipe centerline velocity of $U_{cl} = 5\,\mathrm{m/s}$. The red line indicates the position of the wall obtained by linear fit of the mean velocity profile. Curvature of the inner contour ($R = 500\,\mathrm{mm}$ in the yz-plane is removed.

This distribution is believed to capture the intensity profile of the light sheet as the probability of event-generation increases with increasing light intensity. After reaching a minimum at $y^+ \approx 1.5$ the sample count increases again providing additional measurement data in this domain. The velocity variances, shown in Fig. 10 (b), follow the trends predicted with direct numerical simulation (DNS) by Pirozzoli [7] at a shear Reynolds number of $\mathrm{Re}_\tau = 6000$. The scatter of this data is likely to further reduce when extending the evaluation from $1\,\mathrm{s}$ to the full record length of $30\,\mathrm{s}$.

4.2. Shake-The-Box processing

Shake-The-Box 3d particle tracking was applied to a sample time-series of 4000 images from the CICLoPE dataset. As indicated in Sec. 2.3, application of STB requires certain pre-processing steps to the pseudo-images before they are suitable for processing via iterative particle reconstruction (IPR) and STB. In order to triangulate 3d coordinates of particles, their particle images have to be identified on the images. However, the accumulation of registered events for a single pulse leads to particles being represented as flat-top clusters of various sizes and shapes (see Fig. 11 (a) and (b)). Standard intensity-based peak detection algorithms fail to reasonably identify such particle images as they rely on detecting local maxima. Only small peaks, consisting of single or few active pixels are registered, while the extended flat-top regions belonging to larger particles are not detected (see Fig. 11 (b)).

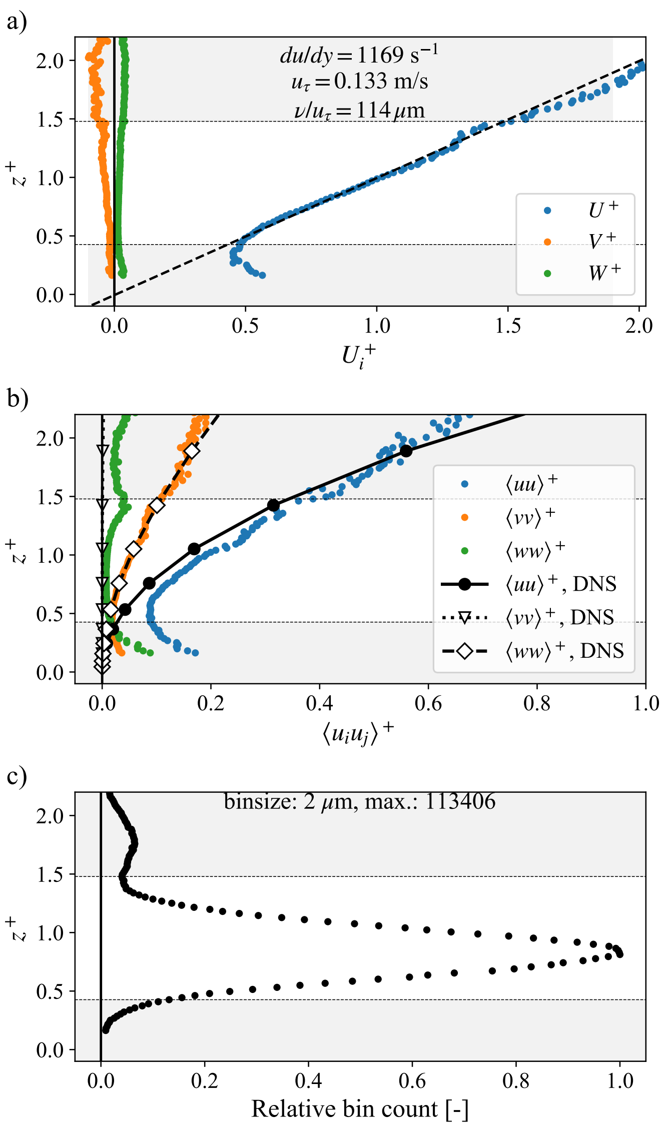

Figure 10. Profiles of the mean (a) and variances (b) of the three velocity components obtained by bin averaging using a bin size of $\Delta z = 2\,\mu\mathrm{m}$. Mean shear rate and associated shear velocity u_τ are estimated from data within the white band ($0.5 < z^+ < 1.5$). Estimated velocity variances are overlaid by DNS prediction for turbuelnt pipe flow at $\mathrm{Re}_\tau = 6000$ [7]. The sample count (c) reflects the intensity distribution of the light sheet.

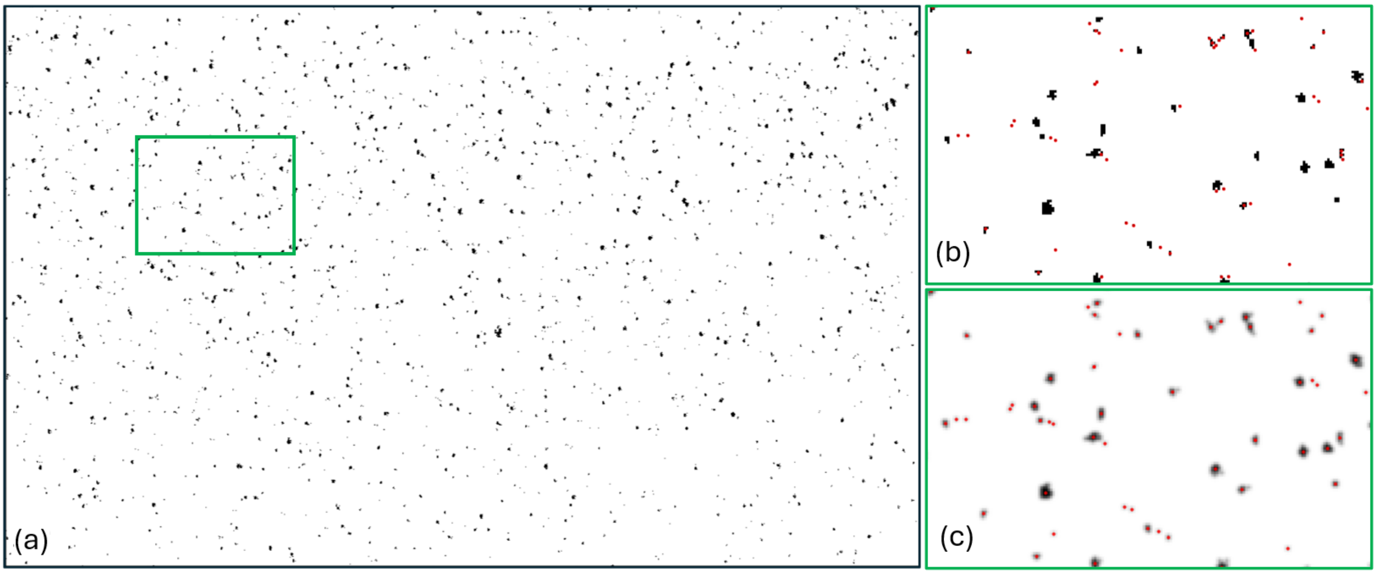

Figure 11. Pseudo-image of a single time-step (a) with zoomed-in inserts without (b) and with Gaussian smoothing (c). Red dots in (b) and (c) show results of peak detection applied to the respective image.

After applying a Gaussian kernel (first application in [5]) with standard deviation $\sigma = 0.8$ pixel (Fig. 11 (c)), the peak detection process is able to reliably detect the centers of such particle images. Weak particle images are sometimes represented as several isolated pixels in the original data and were detected as multiple peaks. After smoothing, the single pixels coalesce into a single Gaussian blob, for which a single peak is found. This demonstrates that the relatively simple technique of Gaussian blurring is capable of transforming the binary pseudo-images into a format where conventional peak detection methods can be applied, however a detailed investigation of the position accuracy of the detected peaks is still to be performed. The Gaussian shape is also a prerequisite for a successful position correction of the 3d particles, which is a key element of the STB processing chain.

The identified peaks are used in a triangulation process to find corresponding 3d particle positions. The required 3d calibration for all cameras is performed as described in Sec. 2.2. The calibrated DLT does not account for lens distortions or other optical effects, e.g. distortions induced by the cylindrical lens used as observation window. To include such effects, a shift field is calibrated for each camera from preliminary STB evaluations: the tracked particles are back-projected to the cameras and the average deviation of the projection point to the actual peak position is determined. Fig. 12 shows the resulting shift fields, gained by averaging all particles located within bins of 60×60 pixels. A clear pattern is visible for both displayed cameras, likely caused by the cylindrical lens. Maximum shifts remain well controlled though, at values below 0.5 pixel.

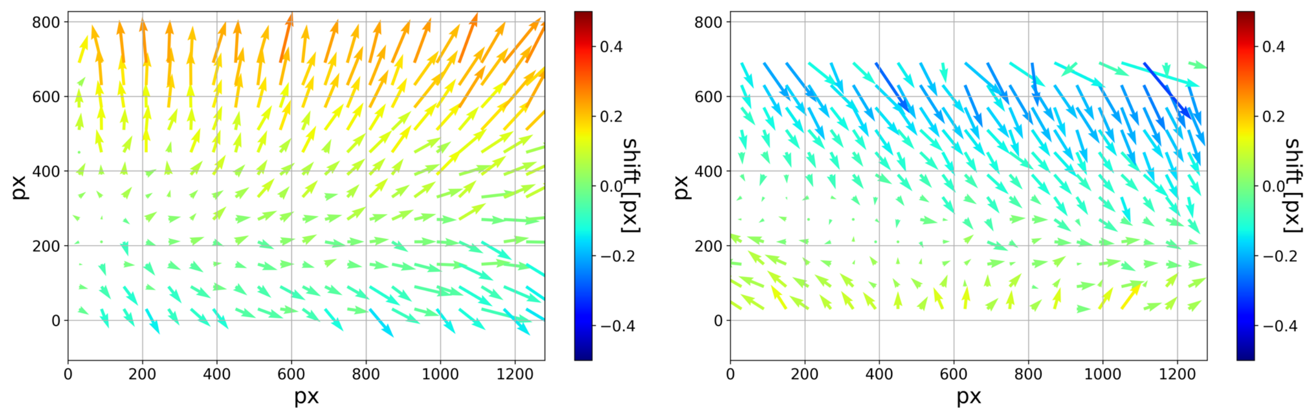

Figure 12. Calibrated shift field applied to the calibration mapping in order to account for optical distortions for two out of the four cameras used. Color-coding by shift in y-direction.

To account for the resulting particle image shape after Gaussian smoothing, a calibration of the optical transfer function (OTF) [12] is performed. Finally, the pre-processed images are used as input for an STB evaluation using the DLR implementation of this algorithm [11]. The images show a low particle image density of around N_I = 0.005 particles per pixel (ppp) – therefore a lean IPR processing can be applied, consisting of a single triangulation with an allowed triangulation error of 1.0 pixel and 3 out of 4 cameras required to register a peak (for details, see paper on advanced IPR, [6]). Depending on the instantaneous seeding density, around 1000-1800 peaks are identified per camera, from which 600-1100 tracks are reconstructed.

Fig.13 compares the post-processed image of a certain time-step to the image created by re-projecting all tracked particles (multiplied by a factor of 2.5) to this camera. The good accordance of the two images (illustrated by the low-intensity residual image) confirms that the majority of particles were successfully tracked.

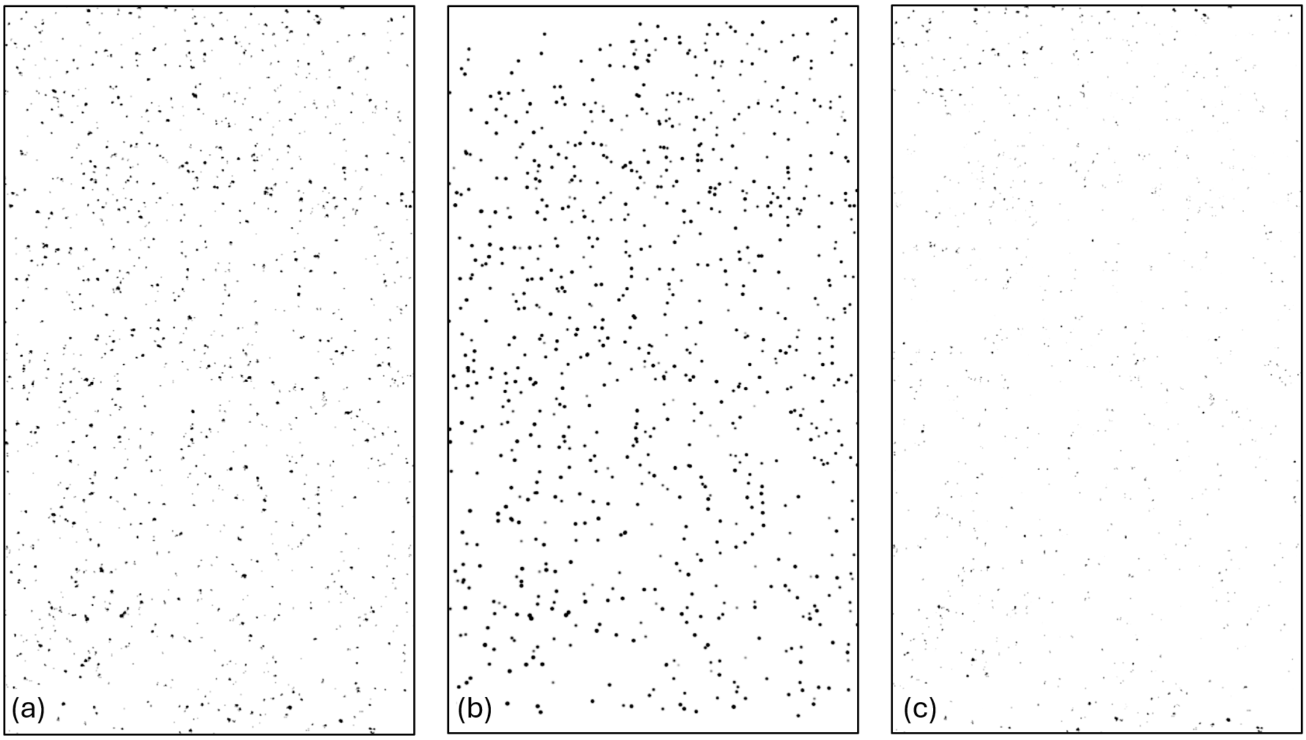

Figure 13. Comparison of Gaussian-blurred pseudo-image (a) to back-projected image of STB-tracked particles (b) and the resulting residual image (c), created by subtracting (b) from (a).

Fig.14 shows an example flow situation, described by around 700 tracked particles, shown over 15 time-steps. The top view reveals a low-speed streak close to a sweep event, where fast fluid is pushed towards the wall. The side and front view show the existence of two clearly separated regions of tracked particles parallel to the wall. This observation is underpinned by Fig.14 (d), showing a density plot of all particles from 1000 evaluated time-steps ($250\,\mathrm{ms}$). In this view a third layer of tracked particles, approx. 0.25 mm above the wall becomes faintly visible. These results are likely caused by an intensity variation of the laser illumination that was generated by an interference of the main beam and a reflection on the pipe wall. The laser intensity in the minima of the resulting intensity pattern is insufficient to provide light scattering by the particles. Also the reduced illumination close to the wall may explain the fact that slow particles are not tracked, in case a high-speed sweep is present above. Slower particles are pushed towards the wall and are lost for the tracking, as they are not well illuminated anymore. This effect can be seen in Fig.14 (a) in the high-speed region from -10 to -5 mm, where low-speed particles are completely missing.

The curvature of the reconstructed bands in radial direction is higher than the local curvature of the pipe wall. This shape is caused by the light reflecting off the curved inner surface (cylinder lens). The effect of this on the calibration remains to be investigated.

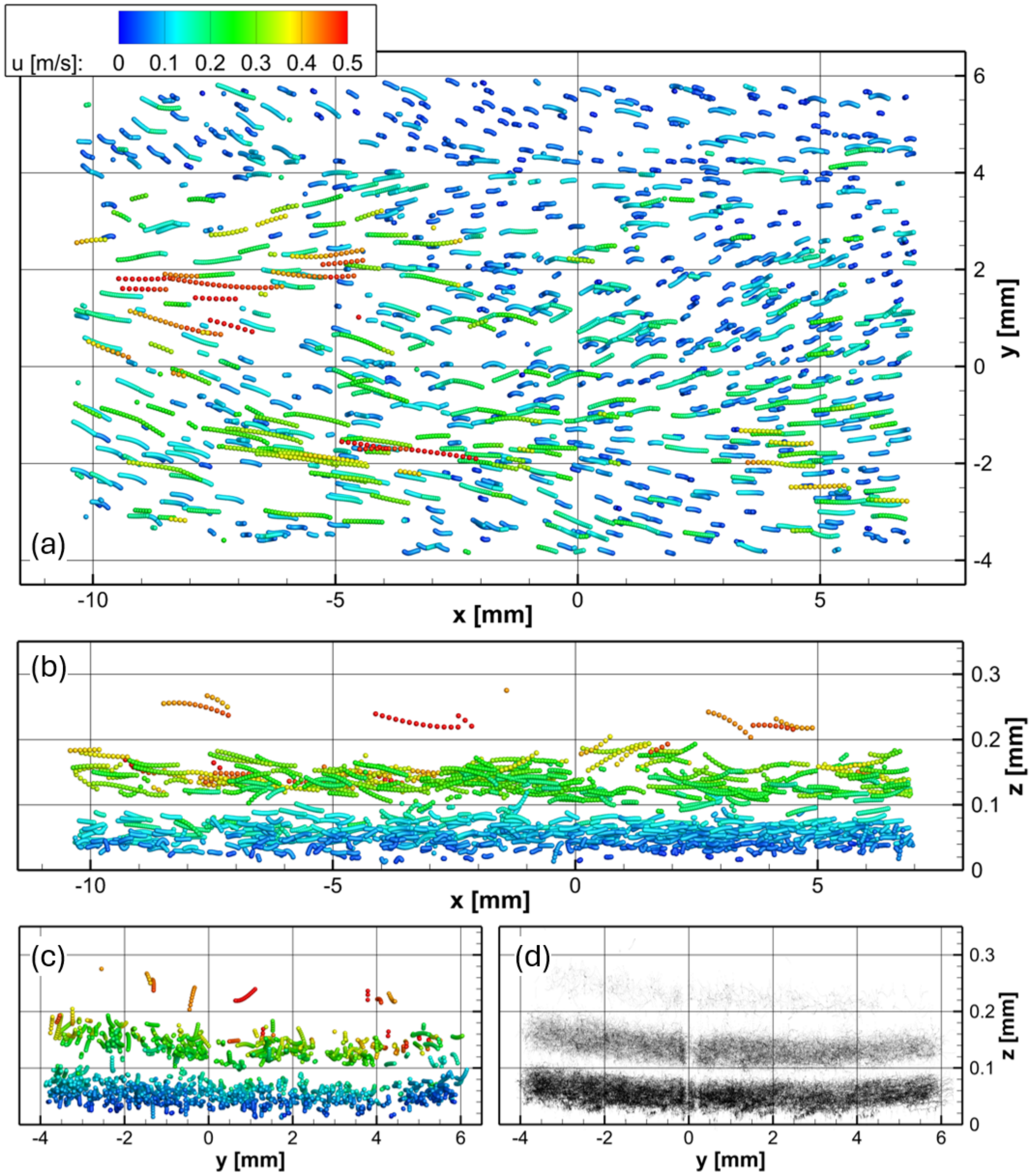

Figure 14. Around 800 particles tracked over 15 example time-steps ($3.75\ \mathrm{ms}$) by STB in the CICLoPE data. Views from top (a), side (b) and front (c). (d) shows front view, with the particles of 1000 time-steps shown as dots to demonstrate the reconstructed stripes, likely caused by inhomogeneous illumination.

All in all, the CICLoPE dataset proved to be suitable for tracking using STB, however, the intensity profile prevents a reliable generation of long tracks. The tracks of particles leaving the illuminated areas are usually retained for a couple of time-steps - albeit at diminishing accuracy, especially in the depth (z-) direction. In order to accurately judge the features and challenges in applying STB to event-based (pseudo-)images, a dataset with homogeneous light conditions would be preferable. Unfortunately, an evaluation of the flat plate TBL-dataset was not feasible due to time constraints.

5. Summary & Outlook

This work demonstrates the feasibility of event-based 3d Lagrangian particle tracking in near-wall turbulent flows using a synchronized four-camera event-based imaging system. To the authors' knowledge, this represents one of the first implementations of a four-event-camera configuration aimed at volumetric particle tracking using the open-source STELLA framework and Shake-The-Box processing in wall-bounded turbulence. Measurements were performed in the viscous sub-layer of both a turbulent flat-plate boundary layer and a turbulent pipe flow. Particular attention was devoted to the CICLoPE Long Pipe dataset, where the large physical scale of the facility enables near-wall measurements at high Reynolds number while preserving spatial resolution in viscous units.

Both continuous illumination and pulsed operation were tested in the pipe-flow configuration using a simple 1 W continuous-wave laser source. The preliminary results show that the tested processing strategies are able to retrieve physically consistent particle motion. The reconstructed tracks reveal near-wall features compatible with the expected organization of wall turbulence, including streamwise-oriented regions of different velocity and signatures of sweep-like motions.

A central processing challenge is posed by the binary nature of event-based pseudo-images, since the flat-top particle images produced by pulsed illumination are not directly compatible with standard peak-detection and STB position-optimization procedures. A simple Gaussian smoothing filter was shown to provide an effective workaround, enabling particle detection, triangulation and tracking with conventional STB processing. In the processed CICLoPE data, approximately 600–1100 tracks were reconstructed per time step, depending on the instantaneous seeding density. However, the accuracy of this preprocessing step and the potential of more event-native approaches still require further investigation.

In the current CICLoPE experiment, inhomogeneous illumination, likely caused by interference between the main beam and wall reflections, produced separated illuminated bands and limited the generation of long, robust trajectories. Improved optical conditions, together with refined preprocessing and calibration strategies, will be needed before quantitative turbulence statistics can be extracted with confidence. The available long-duration recordings, including the flat-plate dataset, provide a valuable basis for this next step, and confirm the suitability of the CICLoPE Long Pipe facility for further development of event-based volumetric tracking in high-Reynolds-number wall turbulence.

References

[1] Bellani, G., Talamelli, A.: The Final Design of the Long Pipein CICLOPE. Springer Proceedings in Physics pp. 205–209 (2016). DOI: 10.1007/978-3-319-29130-7_36

[2] Borer, D., Delbruck, T., Rösgen, T.: Three-dimensional particle tracking velocimetry using

dynamic vision sensors. Experiments in Fluids **58** (2017). DOI: 10.1007/s00348-017-2452-5

[3] Drazen, D., Lichtsteiner, P., Haefliger, P., Delbruck, T., Jensen, A.: Toward real-time particle tracking using an event-based dynamic vision sensor. Experiments in Fluids **51**, 1465–1469 (2011). DOI: 10.1007/s00348-011-1207-y

[4] Gallego, G., Delbrück, T., Orchard, G., Bartolozzi, C., Taba, B., Censi, A., Leutenegger, S., Davison, A.J., Conradt, J., Daniilidis, K., Scaramuzza, D.: Event-based vision: A survey. IEEE Transactions on Pattern Analysis and Machine Intelligence **44**, 154–180 (2022). DOI: 10.1109/TPAMI.2020.3008413

[5] Henning, K., Hilfer, M., Kirmse, T., Boden, F.: Measurement methods fusion and application for fluid-structure coupling analysis using PSP/TSP and event-based-imaging-techniques. In: Dt. Luft- und Raumfahrt Kongress DLRK 2023 (2023)

[6] Jahn, T., Schanz, D., Schröder, A.: Advanced iterative particle reconstruction for Lagrangian particle tracking. Experiments in Fluids **62**, 179 (2021). DOI: 10.1007/s00348-021-03276-7

[7] Pirozzoli, S.: On the streamwise velocity variance in the near-wall region of turbulent flows. J. Fluid Mech. **989**, A5 (2024). DOI: 10.1017/jfm.2024.467

[8] Raffel, M., Beresh, S., Eppink, J., Scarano, F., Schröder, A., Schanz, D., Willert, C.: Recent advances in particle velocimetry (III. Event-based imaging velocimetry) (2026)

[9] Rusch, A., Rösgen, T.: TrackAER: real-time event-based quantitative flow visualization. Experiments in Fluids **64**, 136 (2023). DOI: 10.1007/s00348-023-03673-0

[10] Sachs, S., Jung, S., Kahl, M., Willert, C., Keuper, M., Cierpka, C.: STELLA: A modular framework for SpatioTemporal Event-based Lagrangian particLe trAcking. Experiments in Fluids (accepted, to appear) (2026)

[11] Schanz, D., Gesemann, S., Schröder, A.: Shake-The-Box: Lagrangian particle tracking at high particle image densities. Experiments in Fluids **57**, 1–27 (2016). DOI: 10.1007/s00348-016-2157-1

[12] Schanz, D., Gesemann, S., Schröder, A., Wieneke, B., Novara, M.: Non-uniform optical transfer functions in particle imaging: calibration and application to tomographic reconstruction. Measurement Science and Technology **24**, 024009 (2012). DOI: 10.1088/0957-0233/24/2/024009

[13] Schröder, A., Schanz, D.: 3D Lagrangian Particle Tracking in Fluid Mechanics. Annual Review of Fluid Mechanics **55**, 511–540 (2023). DOI: 10.1146/annurev-fluid-031822-041721

[14] Talamelli, A., Persiani, F., Fransson, J., Alfredsson, P.H., Johansson, A., Nagib, H., Rüdi, J.D., Sreenivasan, K., Monkewitz, P.: CICLoPE — a response to the need for high Reynolds number experiments. Fluid Dynamics Research **41**, 0214070 (2009). DOI: 10.1088/0169-5983/41/2/021407

[15] Wang, Y., Idoughi, R., Heidrich, W.: Stereo event-based particle tracking velocimetry for 3D fluid flow reconstruction. In: A. Vedaldi, H. Bischof, T. Brox, J.M. Frahm (eds.) Computer Vision - ECCV 2020, pp. 36–53. Springer International Publishing, Cham (2020). DOI: 10.1007/978-3-030-58526-6_3

[16] Wieneke, B.: Iterative reconstruction of volumetric particle distribution. Measurement Science and Technology **24**, 024–008 (2012). DOI: 10.1088/0957-0233/24/2/024008

[17] Willert, C.E.: Assessment of camera models for use in planar velocimetry calibration. Experiments in Fluids **41**, 135–143 (2006). DOI: 10.1007/s00348-006-0165-2

[18] Willert, C.E., Franceschelli, L.: Real-time particle image velocimetry using event-based imaging. In: 16th International Symposium on Particle Image Velocimetry (ISPIV 2025). Tokyo (JP) (2025). URL https://elib.dlr.de/215850/

[19] Willert, C.E., Klinner, J.: Dynamic wall shear stress measurement using event-based 3D particle tracking. Experiments in Fluids **66**, 32 (2025). DOI: 10.1007/s00348-024-03946-2